HIPO in-flight performance aboard SOFIA

Edward W. Dunham*[a], Thomas. A. Bida[a], Peter L. Collins[a], Georgi I. Mandushev[a], Ian S. McLean[b], Michael J. Person[c], Erin C. Smith[d], Brian W. Taylor[e], and Saeid Zoonematkermani[a]
[a]Lowell Observatory, 1400 W. Mars Hill Road, Flagstaff, AZ, USA 86001;
[b]University of California, Los Angeles, CA, USA 90095
[c]Massachusetts Institute of Technology, 77 Massachusetts Avenue, Cambridge, MA, USA 02139
[d]NASA Ames Research Center, Moffett Field, CA, USA 94035
[e]Boston University, IAR, 725 Commonwealth Avenue, Boston, MA, USA 02215

ABSTRACT

HIPO is a special purpose science instrument for SOFIA that was also designed to be used for Observatory test work. It was used in a series of flights from June to December 2011 as part of the SOFIA Characterization and Integration (SCAI) flight test program. Partial commissioning of HIPO and the co-mounted HIPO-FLITECAM (FLIPO) configuration were included within the scope of the SCAI work. The commissioning measurements included such things as optical throughput, image size and shape as a function of wavelength and exposure time, image motion assessment over a wide frequency range, scintillation noise, photometric stability assessment, twilight sky brightness, cosmic ray rate as a function of altitude, telescope pointing control, secondary mirror control, and GPS time and position performance. As part of this work we successfully observed a stellar occultation by Pluto, our first SOFIA science data. We report here on the observed in-flight performance of HIPO both when mounted alone and when used in the FLIPO configuration.

Keywords: SOFIA, airborne, instrumentation, commissioning

1. INTRODUCTION

HIPO, SOFIA's High-speed Imaging Photometer for Occultations, is a first-light science instrument for SOFIA that is designed to observe stellar occultations[1] and to carry out other time-resolved photometric work such as extrasolar planet transits and occultations[2] and asteroseismic observations[3]. It is a CCD-based imaging photometer that has been described in several previous papers[4,5,6,7]. It is designed to be able to co-mount on the SOFIA telescope with FLITECAM[8] (the so-called FLIPO configuration) to allow simultaneous time-resolved observations at two optical and one infrared wavelength. Its design also factors in its use as a test instrument for the SOFIA Observatory[9]. Its capabilities for high-speed imaging, precise timing, Shack-Hartmann wavefront sensing, and precise knowledge of its focal plane geometry are of greatest importance in this regard. Figure 1 shows HIPO (left) and FLIPO (right) mounted on the SOFIA telescope in June and October 2011.

HIPO had its first flights in June 2011 in conjunction with the fast diagnostic camera[10] and our first FLIPO flights occurred in October 2011[11]. Additional flights in December 2011 using HIPO and the super-fast diagnostic camera[10] were primarily focused on testing the active mass damping system[12]. These flights were all part of the SOFIA Characterization and Integration (SCAI) flight test program[13]. The scope of this program included characterization of the SOFIA telescope, evaluating the integrated performance of the observatory, and carrying out commissioning observations for HIPO and FLIPO. As a bonus we were also able to observe an occultation of a star by Pluto on our second flight in June. We focus here primarily on the HIPO commissioning work and certain FLIPO commissioning aspects of the SCAI activity, though these areas are closely connected to other telescope and observatory-level behaviors that have broader SCAI implications.

*dunham@lowell.edu; phone 1 928 233-3221; fax 1 928 774-6296; www.lowell.edu

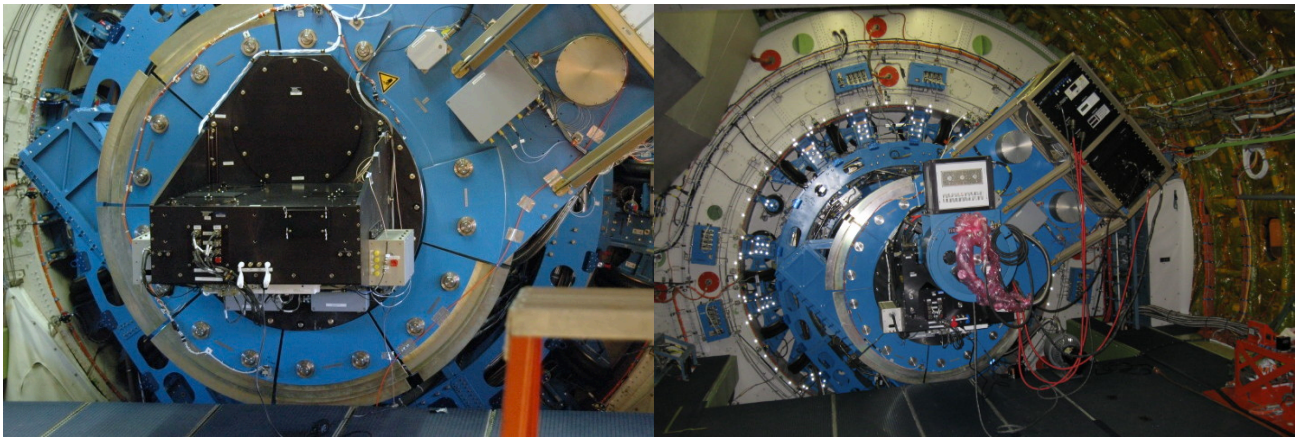

Figure 1. HIPO mounted alone on the SOFIA TA (left) and with FLITECAM in the FLIPO configuration (right). The black anodized HIPO structure is easy to see against the blue TA structure. FLITECAM is blue, nearly the same color as the TA.

The SOFIA Telescope Assembly (TA) is 2.5-meter clear aperture IR-optimized telescope mounted in an open cavity aft of the wing in a Boeing 747SP aircraft[14]. It has a classical Cassegrain optical design with a flat tertiary mirror to fold the optical axis forward along the aircraft's flight axis to its bent Cassegrain or Nasmyth focus. The current flat tertiary has a dichroic beamsplitting coating to allow optical radiation to reach the focal plane imager location. This causes significant light loss for HIPO and the alternative fully aluminized tertiary mirror that is currently being procured in Germany will be preferred for most HIPO uses. Figure 2 shows a side view line drawing of the FLIPO configuration. In this view the tertiary mirror in the TA would be located a considerable distance to the left.

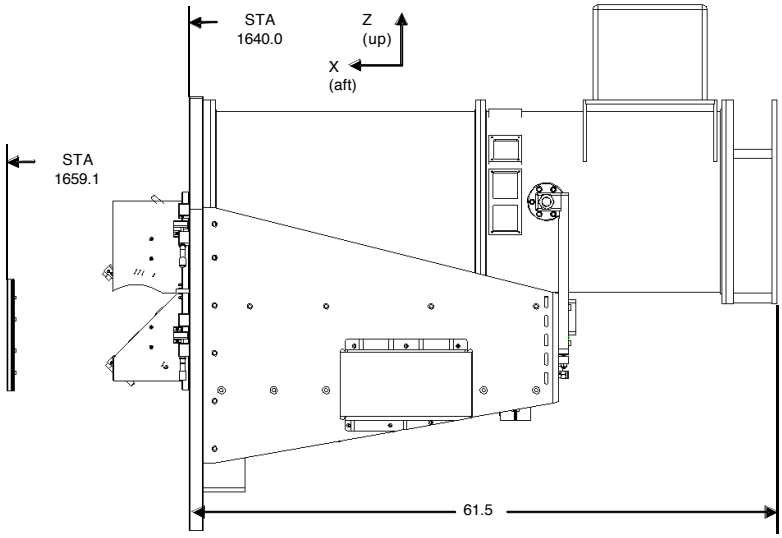

Figure 2. Side view of the co-mounted FLIPO configuration. Light from the telescope enters from the left. The FLITECAM dichroic beamsplitter mounted to the aft face of the main mounting plate at STA 1640.0 transmits optical radiation to HIPO while reflecting the near-infrared radiation to FLITECAM. A silver-coated fold mirror above the beamsplitter completes the optics of the FLITECAM periscope.

The remaining sections of this paper describe the performance of HIPO when mounted to the SOFIA TA. The first section relates to miscellaneous important technical details. The next two sections broadly discuss imaging and photometry, although these two topics are closely interrelated. Finally we describe the occultation observation from a technical and logistical perspective.

2. TECHNICAL UNDERPINNINGS

2.1 Time and position

The HIPO science cases and test work are dependent on precise timing of our observations[6]. For occultation work the position of the telescope is also of central importance. Our ability to satisfy these requirements fundamentally relies on the flight performance of our Trak 8821 GPS clock units. We were able to test our two GPS units against a facility Ashtech unit that was capable of differential GPS accuracy when the aircraft was in the vicinity of the differential GPS base station at Edwards AFB. This test showed that the latitude and longitude provided by the Trak units were in agreement both with each other and with the differentially corrected positions from the Ashtech unit to their level of truncation (0.001 minute of arc) with two exceptions. The first was a period on the SCAI-1 flight during which the Ashtech unit had trouble finding satellites for about an hour. The second exception is that all of the GPS units show short periods with poor performance when a satellite is added to or dropped from the position solution.

Altitude performance was not as good. The Trak units were in perfect agreement with each other but showed an altitude systematically higher than the Ashtech unit by about 100 feet. This value appears to be latitude dependent. We suspect that this discrepancy is due to a small difference between the reference geoids used by the two companies in spite of the fact that both coordinate systems are WGS84. In any case the systematic error meets our positioning requirement.

2.2 Temperature and humidity

We carried out a series of tests related to temperature and humidity due to concern that the HIPO entrance window might develop frost on the face of the window inside the HIPO optical box. The inside window surface is exposed to cabin conditions while the outside face sees stratospheric conditions. It immediately became clear that the window was always within a degree or two of cabin temperature in spite of the direct path to the stratosphere through the TA's Nasmyth tube and the telescope cavity. This suggests that air circulation in the Instrument Flange (INF) is very weak and the air temperature seen by the window is nearly cabin temperature in spite of the insulation on the HIPO mounting plate and the INF's inside surfaces.

This became a larger concern during the FLIPO flights. The thermal background seen by FLITECAM was higher than expected given the measured emissivity (at 3.1 μm) of the optics. The probable high temperature of the 8% emissive FLITECAM entrance window and 12% emissive FLITECAM beamsplitter was presumably a factor. During the December SCAI flights the fold mirror in the FLITECAM periscope was instrumented with a temperature sensor. We found that it, like the entrance window, remained nearly at cabin temperature.

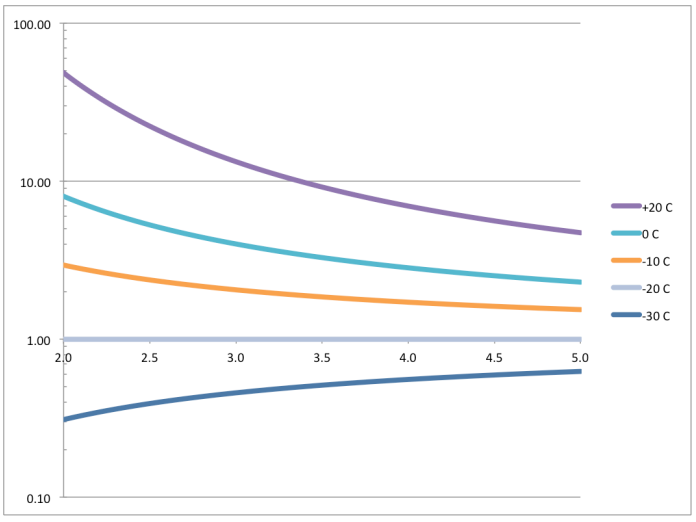

Figure 3. The ratio of FLITECAM's thermal background to the background if the periscope optics and the FLITECAM entrance window were at -20C is shown for several temperatures as a function of wavelength in microns. The measured optics temperature in flight was about +20C (the upper curve). We expect that a temperature of -20C could be achieved using the blower system described in the text. A reduction in background of an order of magnitude in the 3-3.5 micron range can be expected when this system is installed.

A blower system has been designed to circulate stratospheric air through the INF and exhaust it overboard but it has not yet been installed. When installed we anticipate that the optics could realistically reach a temperature of -20C given a

cavity recovery air temperature of -30C. Figure 3 shows the thermal background as a function of wavelength for several assumed temperatures relative to the background at -20C. The large factors at wavelengths below 2.5 µm are not relevant since the actual value of the thermal emission is low there, but thermal background dominates at wavelengths beyond 2.5 µm. Improvement of an order of magnitude can be expected at 3-3.5 µm, decreasing somewhat to the 5 µm cutoff of FLITECAM's InSb detector.

Further improvement can be expected if a good AR coating can be found for the FLITECAM CaF_2 entrance window and a better dichroic coating for the FLITECAM beamsplitter can be obtained.

2.3 Cosmic rays

Experience with the Kuiper Airborne Observatory (KAO) suggested that the rate of cosmic ray hits in flight would be much larger than seen at ground-based observatories[15]. For the purposes of this evaluation we focused attention on the 1Kx1K CCD47-20 detectors, not the CCD67 we flew in the blue channel on the last seven flights. We monitored cosmic ray hits during climb and descent legs as well as during turns and other times when HIPO was otherwise not engaged. For commissioning purposes we defined an affected pixel to be a pixel 5σ above the background in a bias-subtracted and overscan corrected 60-second dark frame and simply counted the number of affected pixels in each dark frame. The intrinsic dispersion (max/min) in the cosmic ray rate was found to be close to a factor of two although there were typically several hundred affected pixels per frame. This suggests that the observed hits were due to secondary cosmic rays from much less numerous primary cosmic rays incident on the atmosphere.

The roughly exponential altitude dependence of the cosmic ray rate is shown in Figure 4. The trend of the line corresponds to a factor of 10 increase in cosmic ray rate per 7 km of altitude. We also found evidence for a weaker dependence of cosmic ray rate on latitude by looking at the lowest-latitude points on SCAI-2 (+ 24 degrees as part of the Pluto occultation) and highest latitude points (+63 degrees on SCAI-9) and all the points at intermediate latitudes that fell between the altitudes of the SCAI-2 and SCAI-9 points, taking into account the altitude dependence just measured. The high latitude rate was roughly a factor of two higher than the low latitude rate. Given the intrinsic dispersion in the rates and the very different dates of the two flights this dependence cannot be considered to be well established.

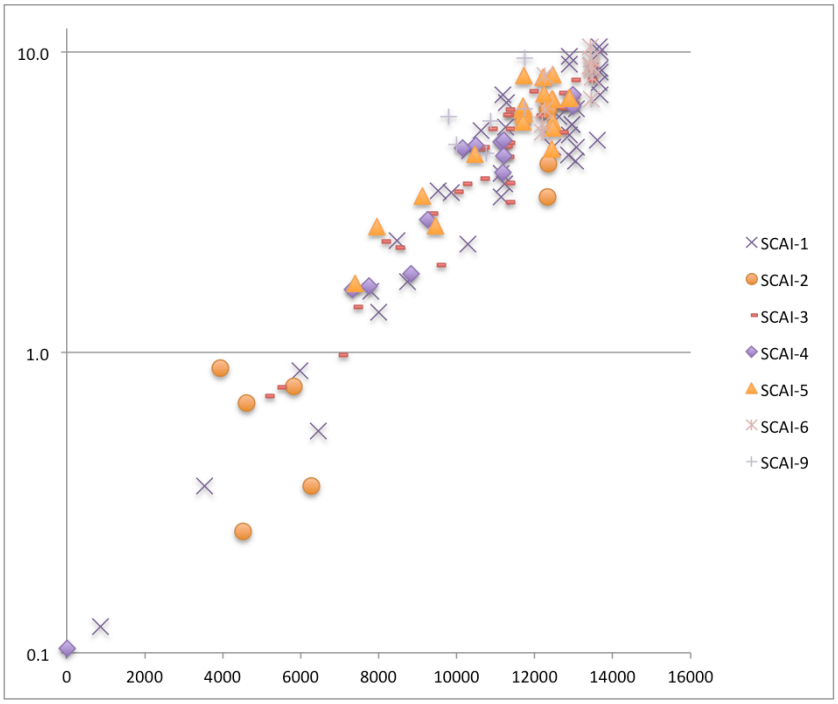

Figure 4. The rate of affected pixels (in units of pixels/sec/cm^2) plotted against HIPO GPS altitude in meters. The exponential dependence and ~2x scatter described in the text are clearly seen.

We also generated the histogram of signal levels in the affected pixels, seen in Figure 5. This shows a power law dependence with an index near -2, with many more low signal hits than high signal ones. There are clearly many more events at lower levels that did not cross our 5σ threshold, but these will have little impact on our scientific observations.

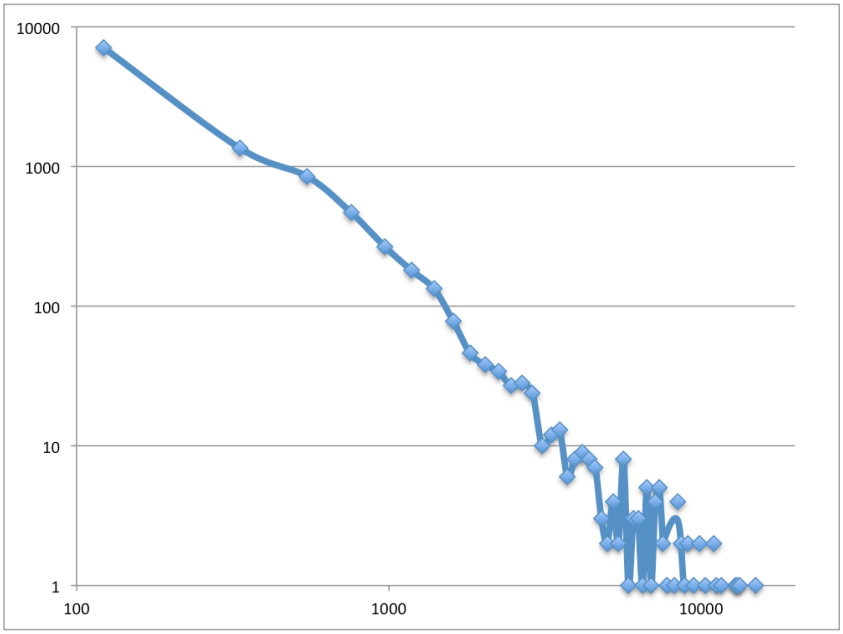

Figure 5. The rate of affected pixels (on the vertical axis in units of pixels/sec/cm^2) plotted against the pixel value expressed in electrons on the horizontal axis. This shows a power law dependence with an index close to -2.

2.4 Readout mode performance

The various HIPO readout modes are described in detail in our 2008 paper[6]. Since that time we have added the capability to observe using a NIMO e2v CCD67 that has both very much faster parallel clock speed and fewer pixels than our normal AIMO CCD47-20 sensors[7]. We flew a CCD67 on the HIPO blue side for the October and December flights in order to make high frequency measurements of the telescope's vibrational image motion.

The highest speed continuous data acquisition mode we have is the pipelined occultation mode[6]. Using the CCD67 with an optimally placed subframe, binning 2x2 for an image scale of 1.3 arcsecond per binned pixel, and using a fast but noisy readout speed we were able to achieve the frame rates and subframe sizes listed in Table 1.

Table 1. CCD67 subframe sizes, locations, and frame rates.

Subframe size (“)	Subframe size (pixels)	Subframe center (binned pixels)	Frame interval (μs)	Frame rate (Hz)
16x16	12x12	(9,6)	370	2702
20x20	15x15	(10,8)	510	1961
25x25	19x19	(12,10)	730	1370
35x35	26x26	(16,13)	1220	820
59x59	44x44	(25,22)	3000	333

We found the best tradeoff between subframe size and frame rate given the observed jitter amplitude and frequency as well as our ability to point the TA precisely, was usually the 19x19 pixel subframe case at 1.37 KHz frame rate.

2.5 Internal jitter

One of the most demanding design requirements for HIPO was its stiffness. This was imposed because of the very tight pointing stability requirement initially imposed on the SOFIA TA, 0.2" rms. As a result we required flexure to be less than 0.1" referred to the sky and required the lowest resonant frequency in the instrument to be greater than 100 Hz[5]. The lowest frequency is in fact 96 Hz, the resonant frequency of the blue fold mirror. The 100 Hz requirement was based on the finite element model of the telescope during development and we have learned since then that the TA has some higher frequency modes of interest.

To ensure that HIPO itself was not contributing significantly to the observed image motion we created a simple test jig to place an LED-illuminated pinhole in the focal plane of the telescope on the HIPO blue side, where all our jitter measurements were made. This simple fixture was mounted to the blue field lens mount. The resonant behavior of the blue fold mirror was measured using this system by plucking the mirror mount like a guitar string. This test revealed a resonant frequency of about 120 Hz and a 250 ms 1/e damping time but with a very small maximum amplitude, 0.25" peak-to-peak. The amplitude spectrum (the square root of the power spectrum) of the motion seen in this test is shown in Figure 6.

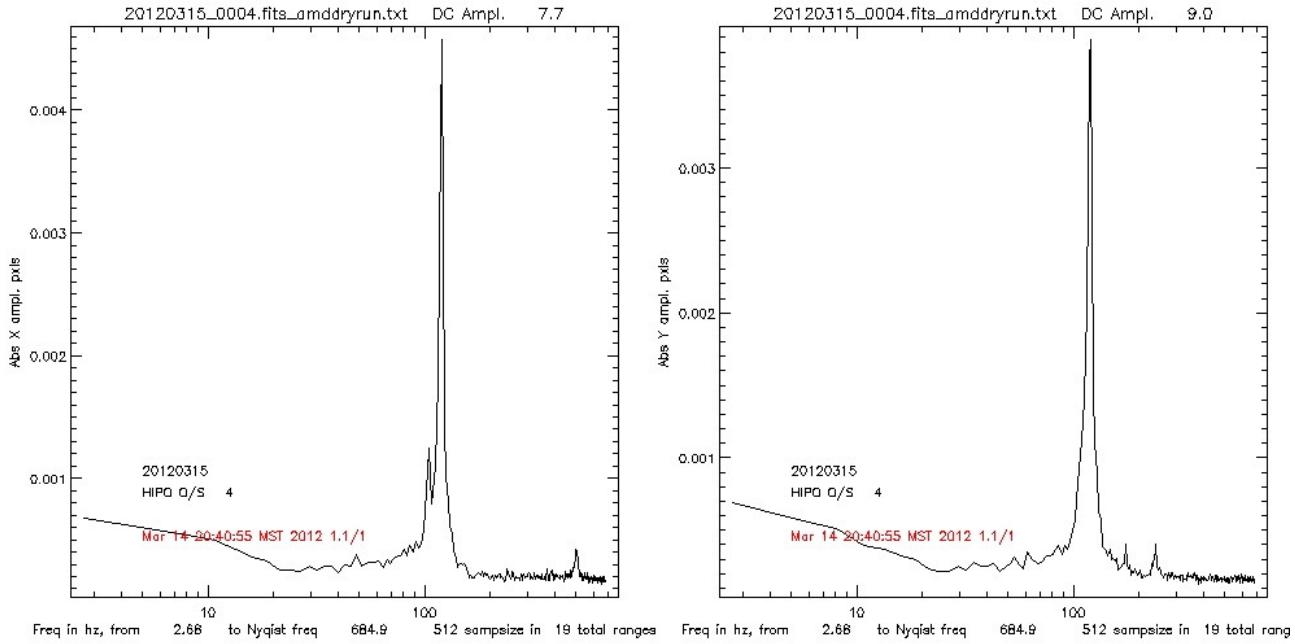

Figure 6. Amplitude spectra of the HIPO blue side fold mirror resonant frequency test described in the text. Although the resonance is pronounced the maximum amplitude is only 0.25" peak-to-peak.

Observations of the test fixture were taken in flight during climb, while the door was opening, and in level flight. A representative in-flight amplitude spectrum of the HIPO X and Y positions is shown in the upper two panels of Figure 7. This dataset was obtained during SCAI-9 at an altitude of 35500 feet about 10 minutes after opening the cavity door. Again, strong resonances are seen but the rms amplitude of the motion is only 0.13" in the X direction and 0.09" in the Y direction. Figure 7 also shows the amplitude spectrum of the image FWHM and the measured flux. In this case, where the LED-illuminated pinhole in the focal plane is the target, these are impacted only by image jitter. When the target is a star the FWHM reveals the primary mirror astigmatic mode at 175 Hz[12]. The spectrum of the measured flux is more difficult to interpret in the case of a stellar target.

We conclude that the expected blue fold mirror resonance is present but has no practical effect because of its small amplitude.

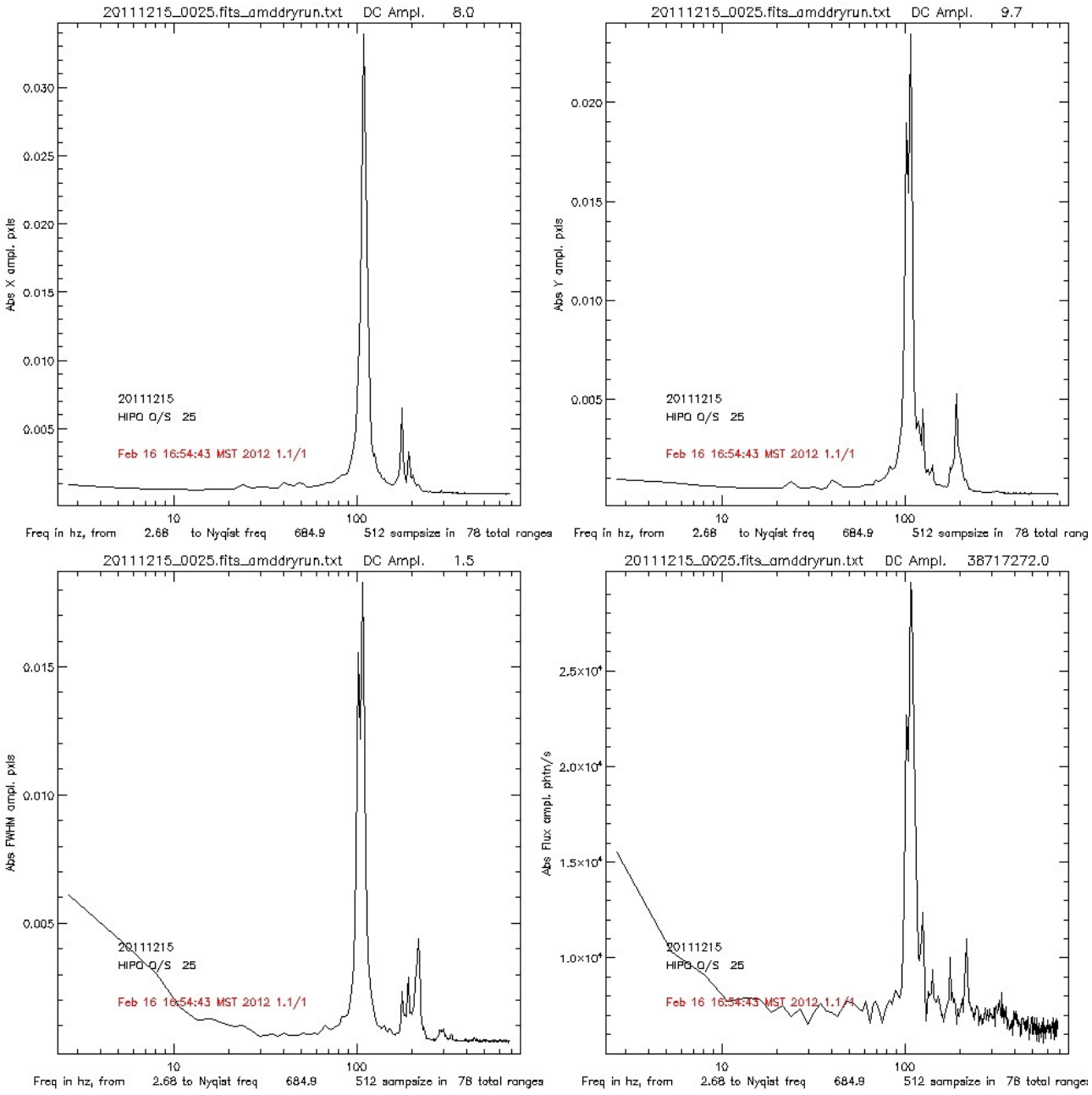

Figure 7. Amplitude spectra of the HIPO blue side fold mirror with the door open in flight. Although the resonances are pronounced the rms amplitude is only 0.13" in the X direction and 0.09" in the Y direction.

3. IMAGING

3.1 Focus sensitivity

The optical prescription of the SOFIA TA includes a very large secondary mirror magnification. This has the result that the focus is highly sensitive to thermal expansion of the metering structure. This obviously has a significant influence on the image size, and less obviously on the photometric flux seen in an electronic aperture used for CCD photometry. This latter effect will be discussed further in section 4.4.

Because of the TA's strong focus sensitivity we devoted considerable effort with the HIPO Shack-Hartmann test capability to establish a well-defined temperature-dependent focus correction. For the purposes of this paper it is sufficient to note that this effort was successful and this calibration is being incorporated into the SOFIA flight software. For imaging purposes the focus should be kept up to date with temperature to a tolerance of about 1 degree C but a tighter tolerance may be needed for the precise photometry application discussed in section 4.4.

3.2 Image motion

Image motion faster than the timescale of an astronomical integration time, which we call jitter, is a significant contributor to the image quality budget. Early flight tests have shown that the dominant jitter contribution is one that was not originally envisioned, a mode involving the secondary mirror, the spider structure, and the baffle plate mounted on the metering structure opposite the Nasmyth tube[12]. To date the active mass damper approach has not been successful in alleviating this vibrational mode. However wind loading on the baffle plate is the source of the energy exciting this mode and removing the baffle plate, as we did for SCAI-9, effectively eliminates this mode. In the near term SOFIA science flights will be flown with the baffle plate removed. Additional time will be needed to develop a modified baffle plate and an operational active mass damper system to mitigate the various primary mirror modes[12].

3.3 Image size and shape

One of the SCAI tests was to examine the size and shape of the stellar PSF as a function of exposure time and wavelength across the HIPO range. This test was guided by our KAO experience[16] and understanding of the SOFIA systems. The primary factors in the optical image size budget are image blur due to shear layer turbulence, image jitter, and defocus. The SOFIA optics are of good quality and are well aligned, and diffraction is negligible at optical wavelengths. At this stage of the SCAI analysis a question remains regarding the relative importance of shear layer seeing and "dome seeing" due to thermal imbalances in the TA cavity.

The jitter components of the image quality budget are now well understood[12] and jitter can be removed from the problem by taking short exposures. We now know the temperature dependence of focus so ambiguities in this regard can also be resolved. Since we were determining this dependence during the SCAI flights some of the images are necessarily not well focused and care must either be taken to avoid them or the focus blur component must be accounted for.

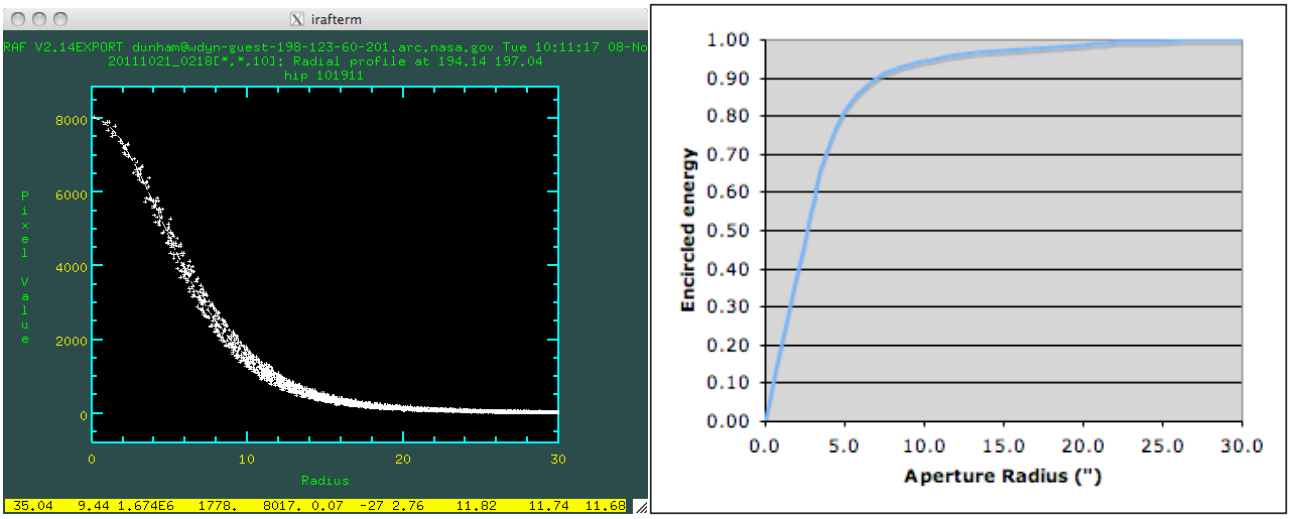

Figure 8. Radial profile (left) and encircled energy (right) of a typical SOFIA image. This is a 1 second R filter exposure in good focus taken at an altitude of 40,400 feet. The horizontal axis of the radial profile is in pixels at 0.327"/pixel.

A comprehensive analysis of this test has not yet been done but the main results are evident. The shear layer component of the SOFIA images is similar to the KAO case. The images are broad and smooth with very broad wings and a FWHM that decreases with altitude. We expect that the PSF shape will turn out to be the Fourier transform of the Kolmogorov optical transfer function that is proportional to $\exp(-f^{5/3})$ as it was on the KAO[16]. The SOFIA PSF shape is

illustrated in Figure 8. The encircled energy has been normalized to unity at a 30" aperture radius but we expect from our KAO experience that this is not really correct. There was noticeable flux outside of a 90" aperture in that case[15] and we expect SOFIA images to behave the same way.

One surprise we have noted is that the SOFIA images do not appear to break up into speckles at very short (200 μs) exposure times like the KAO images did. This may turn out to be the result of spatial resolution that is inadequate to resolve the smaller and probably more numerous SOFIA speckles. Sample images at several short exposure times taken with the fast dots mode[6] are shown in Figure 9.

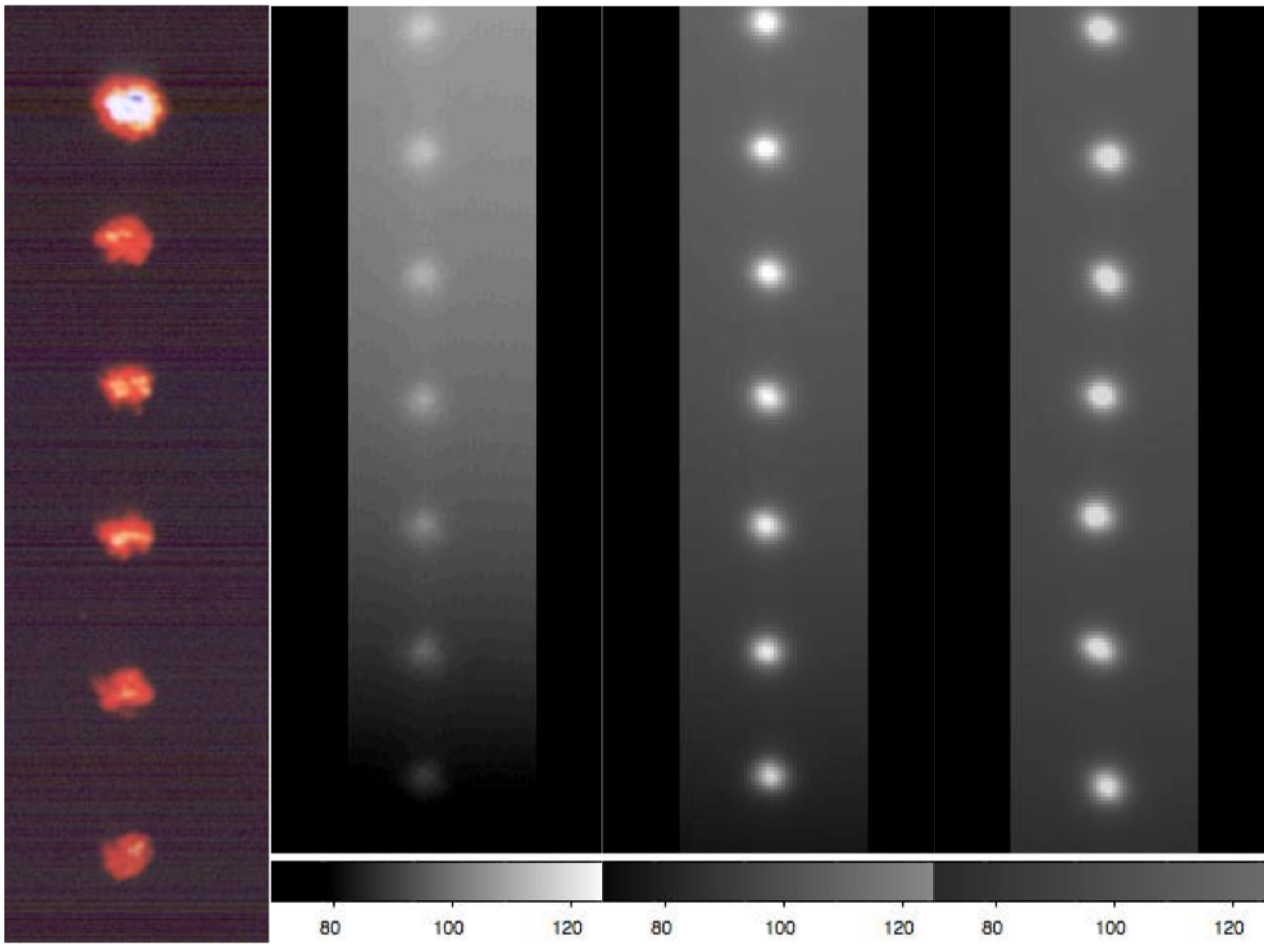

Figure 9. Short exposure images taken in fast dots mode. Individual images in the time series are arranged vertically with the first image at the bottom. From left to right these images are KAO, 500 μs, and SOFIA, 200 μs, 1 ms, and 2 ms exposure times. Note the speckles in the KAO image and the image motion evident in the 2 ms SOFIA image set.

4. PHOTOMETRY

4.1 Throughput

We have made several ground-based attempts to measure HIPO's throughput using observations of spectrophotometric standard stars[5,6,17]. These met with some success but the standard star measurement always indicated a lower throughput than the "bottom-up" approach we use in our sensitivity spreadsheet that accounts for transmission and reflection efficiencies of each surface as well as the quantum efficiency of the detector. We attributed this discrepancy to differences in the way astronomers and reflectometers treat scattering from the coatings of telescope mirrors[6].

During the SCAI-1 flight we had an opportunity to repeat this measurement with SOFIA. Our effort to measure atmospheric extinction in flight was not successful but the measurement of our spectrophotometric standard, Feige 110, was successful. We have assumed atmospheric extinction values based on ozone absorption and Rayleigh scattering at altitude until we have another opportunity to measure the extinction. The reflectivity of the telescope optics was measured less than a week before our in-flight measurement was made. The result of the SCAI-1 standard star test is summarized in Table 2 in the context of previous lab and ground tests.

The first three data columns in Table 2 are the bottom-up prediction and two lab measurements of the integrated transmission of the internal HIPO optics. The agreement between these is very good and gives confidence in this part of the bottom-up calculation. The last three columns represent the ratio of the standard star measurement to the bottom-up calculation. The first two of these represent tests using the Perkins 1.8-m telescope at Lowell and the last is the SCAI-1 test. In all cases the telescope optics reflectivity was measured, but the condition of the primary mirror's coating in 2006 was poor. It was realuminized in 2007 and the O/C agreement was better when the coating was in good condition. The SCAI-1 test O/C agreement in the V filter is somewhat better than the 2007 test and is about the same in the I filter. The R filter is split by the internal HIPO dichroic reflector so the blue and red channel values are both given.

Table 2. HIPO throughput measurements.

Filter	Lab (predicted)	Lab (2005)	Lab (2007)	1.8-m O/C (2006)	1.8-m O/C (2007)	SOFIA O/C (2011)
B	78%	72%	- - -	- - -	- - -	75%
V	76%	69%	72%	63%	75%	85%
R	82%	81%	- - -	- - -	- - -	77% & 96%
I	82%	79%	80%	54%	62%	60%

At first there was a more serious discrepancy between the top-down and bottom-up throughput measurements but this was largely resolved by better data on the transmission and reflection of the dichroic tertiary mirror coating, kindly arranged by P. Waddell. The low reflection coefficient of the tertiary mirror at optical wavelengths, shown in Figure 10, explained most of this poor agreement. High transmission to the focal plane imager at optical wavelengths is desired for normal IR operations that depend on the focal plane imager but it is a serious blow to HIPO, which is why we prefer to use the aluminized tertiary mirror.

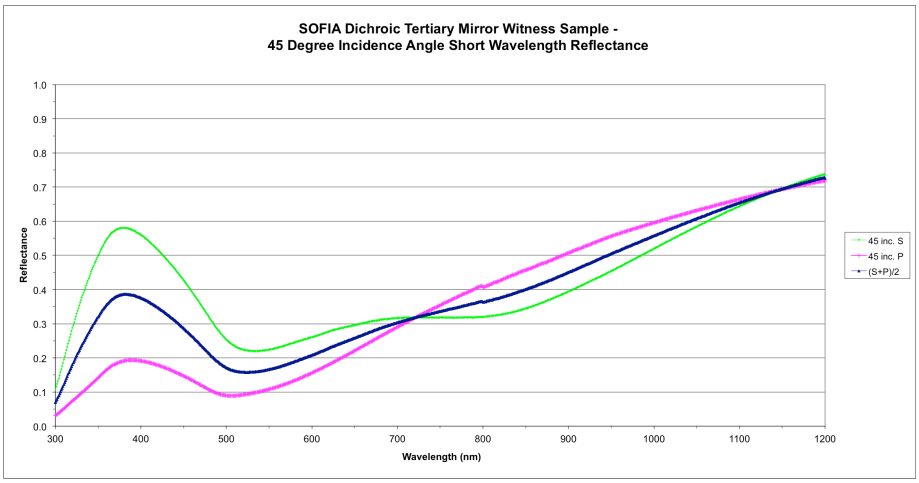

Figure 10. Measured reflection coefficient of the SOFIA dichroic tertiary mirror across the HIPO wavelength range at the operating 45 degree angle of incidence. The low reflectivity is a serious problem for HIPO. The polarization sensitivity was unexpected.

Another weak point in the throughput of HIPO is the FLITECAM dichroic beamsplitter used in the FLIPO configuration. Very roughly it has a 50/50 transmission/reflection ratio in the HIPO bandpass and 88% reflectivity (and more importantly 12% emissivity) at 3.1 microns, a typical FLITECAM wavelength. The SOFIA dichroic tertiary serves as an obvious existence proof that better coatings are possible. Improving this beamsplitter is an active work area.

4.2 Twilight sky brightness

Occultation observations are frequently complicated by small solar elongation angles that force observations to occur in or near twilight. We made some measurements as part of the SCAI flight series in the spirit of Dunham and Elliot's KAO measurements 35 years ago[15]. We were successful in measuring the sky brightness as a function of solar elevation angle with results that were similar to the KAO results but our coverage in azimuth was less than perfect. Also, as in the KAO measurement, we have little or no understanding of the effect of the elevation angle of the observation. This has led to the development of a test plan that should provide a much more thorough test in a short amount of flight time.

4.3 Scintillation

We expect SOFIA photometry to show very low scintillation noise, perhaps none at all. This is based in part on our KAO experience[15], in part on the study of scintillation at ground-based sites[18], and in part because the physical mechanism causing ground-based scintillation (high altitude turbulence) occurs *below* our observing altitude. We made several scintillation measurements during the SCAI flight series. In each case we obtained a number of basic occultation time series on the order of one minute long with time resolution of 0.1 or 0.2 seconds.

Analysis of this data is ongoing but some early results are clear. The scintillation data are of course at very high signal to noise ratios (SNR) and are sensitive to jitter effects and to the long-term drifts discussed below in the precise photometry section. We need to reject the low signal outliers that occur when jitter causes flux to be lost from our aperture and we fit linear trends to each time series to remove the slow drifts. In some cases these corrections make a noticeable difference in the resulting SNR but in other cases no significant change is seen. We have seen noise levels as low as 1/3 of the noise expected from the combination of Poisson noise and ground-based scintillation extrapolated to flight altitude, but we have not seen noise levels as good as pure Poisson noise. Work to search for correlations with possibly relevant parameters is underway. We will also explore the possibility that we are witnessing near-field scintillation from turbulent structures in the shear layer. This is usually discounted because of the short propagation distance from the shear layer to the telescope's entrance aperture but the combination of strong turbulent density fluctuations (relative to the much more benign ground-based case) and high SNR may make this a significant effect.

4.4 Precise photometry

The study of extrasolar planet transits and occultations (primary and secondary minimum in variable star terminology) requires very precise photometry, on the order of 0.01%, over periods of hours. While this is technically very challenging the scientific payoff can be very high[2] and there is intense interest in finding a way to make this work.

We undertook precise photometry test measurements on SCAI-6 and SCAI-9. Our first attempt was in the FLIPO configuration and used a reference star out of our field of view that required small telescope motions to observe. Our second attempt used HIPO and the SFDC[10] with a reference star in the field of view. In both cases the data were corrected with bias frames, overscan columns, and flat fields. The raw photometry (i.e. not differentially corrected using the reference star) showed variations on the order of several millimagnitudes on a timescale of 15 minutes or so. These variations had similar character on the HIPO blue and red sides and in the SCAI-9 test the SFDC saw the same behavior as well. At this time the FLITECAM data do not have sufficient SNR to resolve these drifts.

Figure 11 shows the relative photometry (by this we mean photometry relative to its mean value, not relative to another star) seen during the SCAI-6 test. In this figure the red side photometry is in the left panel and the blue side is on the right, the vertical axis is the fractional deviation of the photometry from its mean value, and the horizontal axis is elapsed time in minutes. The points are average values of 1-minute datasets. Each curve corresponds to a different aperture diameter with the smallest aperture diameter (15.4" and 13.1" for the red and blue sides) being at the bottom and the largest (46" and 34" for the red and blue sides) at the top. The individual aperture curves are offset vertically by 0.002 for clarity. Figure 12 shows the red and blue data for the SCAI-9 test. Here the "target" star was HD85216 and the "reference" star was its nearby and fainter neighbor, BD+19 2271.

The similar character of the variation in the two sides can be seen in Figures 11 and 12, while Figure 11 also shows that the amplitude of the variation decreases as the aperture diameter increases. We conclude that the variation is not primarily instrumental in nature and is likely to be due to the wings of the broad PSF interacting with the edge of the aperture. The strong influence of image position seen in *Kepler* photometry is not seen here and our best present understanding is that these variations are due to small changes in the size and shape of the PSF.

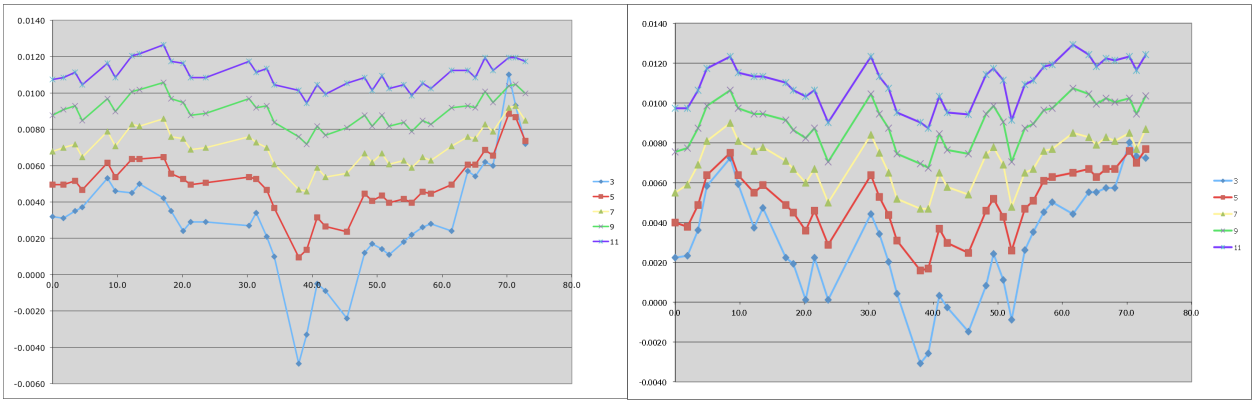

Figure 11. Relative photometry as a function of elapsed time (in minutes) seen during the SCAI-6 precise photometry test.

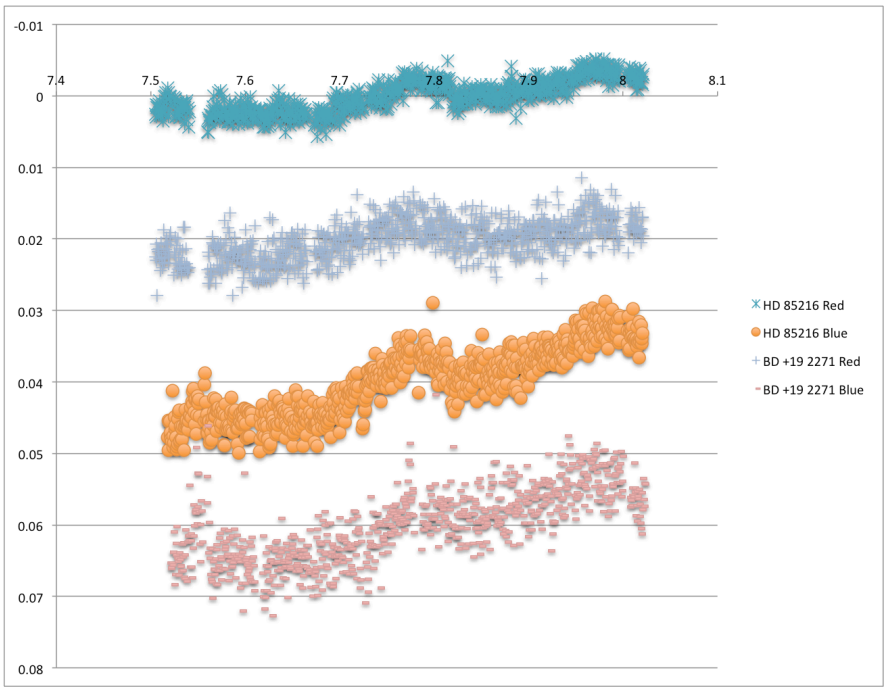

Figure 12. Relative photometry as a function of UT in fractional hours seen during the SCAI-9 precise photometry test. From top to bottom the curves are the red and blue side data for the "target" star and the bottom two curves are the red and blue side data for the "reference" star. The curves are offset for clarity.

The three factors that primarily influence the image size and shape, jitter, focus, and shear layer turbulence, obviously must be relevant here as well. It is important to note that the baffle plate was not installed during SCAI-9 flight and the jitter contribution was significantly reduced because of this. If anything the variation during the SCAI-9 test is larger than in the SCAI-6 test so we conclude that jitter is not the primary source of trouble. Focus was adjusted several times during the SCAI-6 test to keep up with slow temperature drifts but the temperature during the SCAI-9 test was stable enough that we did not change the focus. This leads us to consider the shear layer contribution.

The image size produced by the shear layer is proportional to the rms density fluctuations in the shear layer and the thickness of the shear layer, and is inversely proportional to the integral scale size of the turbulent structures[16]. The shear layer thickness and turbulent scale size are not likely to change significantly under typical flight conditions, but the rms density fluctuations likely will[19]. In fact they are proportional to the square of the Mach number and to the mean free-air density. As a result the image size and photometric signal will change with Mach number, altitude, and free-air temperature. It is possible to estimate the expected magnitude of these effects by using the encircled energy curve (Figure 8) and understanding the degree to which Mach number and altitude can be controlled by the flight crew.

We have made these estimates and variability on the order of a few millimagnitudes can be expected to occur in normal flight. The overall slope in the SCAI-9 data is consistent with the steadily increasing altitude of the aircraft during the test (from 40640 to 41012 feet) combined with atmospheric extinction (the field was rising and the airmass decreased by 0.16 during the test). We interpret the variations on shorter timescales as being due to Mach number changes on the order of 0.01. Unfortunately Mach number could not be logged during the SCAI flights. The relatively more stable SCAI-6 data were taken at a nearly constant altitude and the airmass change during the observation was only 0.03.

Additional flight data will be logged and archived during the next series of flights and the resolution of these data appears to be sufficient to apply post-facto corrections to the photometry to remove these effects. We have planned a test to vary the several parameters of interest to calibrate their impact on our photometry.

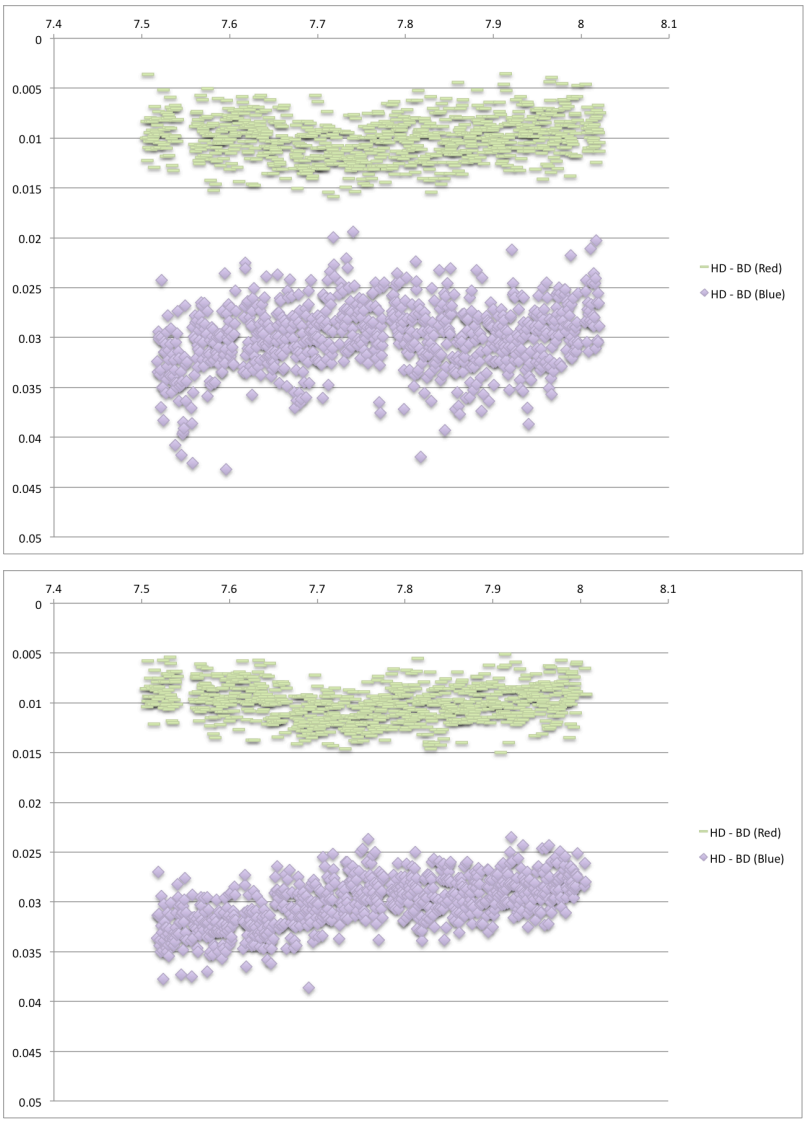

Figure 13. Differential photometry for the SCAI-9 precise photometry test. The magnitude difference between HD85216 and BD+19 2271, normalized to a mean of zero and offset for clarity, is shown for the HIPO red data (top) and blue data (bottom) in each of the two panels. The upper panel used a larger photometric aperture (19.4" and 26.2" diameter for the blue and red data, respectively). The lower panel used smaller apertures, 16" diameter for both red and blue data.

So far we have considered only the raw photometry. Next we consider the differential photometry that was possible with the SCAI-9 data set. Figure 13 shows the magnitude difference between HD85216 and BD +19 2271 with two different aperture sizes. The apertures used for the photometry in the upper panel were larger (19.4" and 26.2" for the red and blue data) while those in the lower panel were smaller (16" diameter for both red and blue data). Several points

stand out. First, differential photometry is not a cure-all for long-term instability. While the differential photometry is far more stable than the raw photometry it still shows low-frequency trends at levels unacceptable for transit work. Second, the photometry using the larger aperture is more stable on the long term but has more scatter while the smaller aperture has less scatter and more instability. Clearly this is pointing to an optimization between larger apertures to reduce the magnitude of required corrections and smaller apertures to reduce the noise from the background with the goal of minimizing the noise seen on timescales of interest to the observation in question.

5. PLUTO OCCULTATION

As part of the SCAI flight series we had the opportunity to observe a stellar occultation by Pluto on 23 June 2011 UT as part of the SCAI-2 flight. The flight plan out over the Pacific Ocean is illustrated in Figure 14. As the flight proceeded occultation prediction astrometry data were being obtained with the US Naval Observatory 1.5-m telescope in Flagstaff (represented by a red dot in the figure). These images were transferred to MIT (the next red dot) where they were analyzed in real time. An Iridium satellite (third red dot) phone call was placed to the SOFIA flight deck (last red dot) in time to update the flight plan so that we could target the aircraft as close as possible to the center of the occultation shadow. By this process we were able to observe the event from a location only 100 km from the center of the occultation shadow path. This corresponds to an astrometric error of only 0.0046", a feat that would have been impossible without the in-flight prediction update.

We look forward to carrying out further targeted occultation observations with SOFIA in the coming years. The development of this capability is particularly timely given the impending flyby of Pluto by New Horizons.

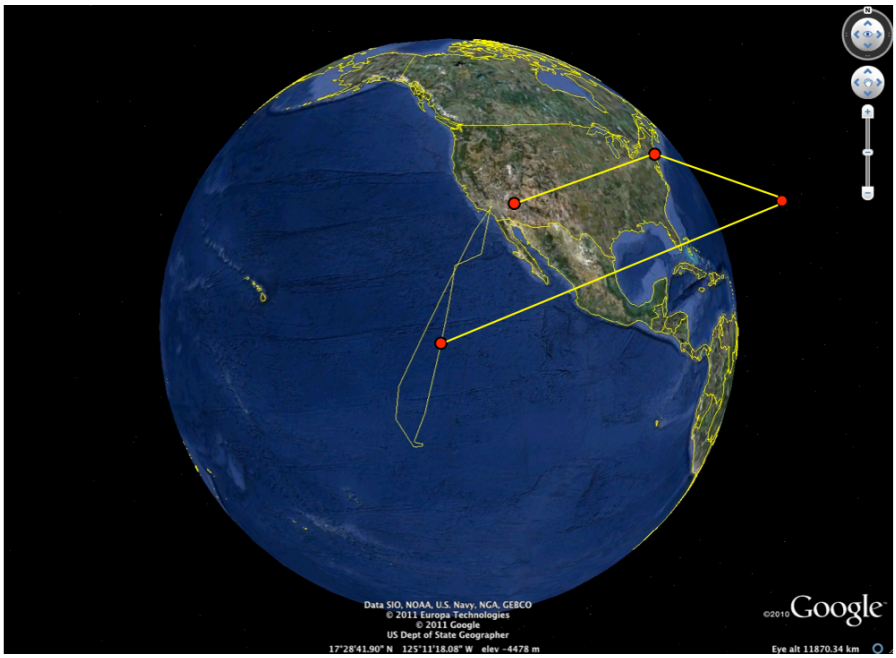

Figure 14. The SCAI-2 flight plan is shown as the long, looping path out into the Pacific Ocean and back. An early calibration leg on Pluto occurred off of Baja California and the occultation occurred on the short leg at the far end of the flight plan. The red dots and yellow lines refer to the in-air occultation prediction update. See text for further discussion.

6. SUMMARY

This is an exciting time for SOFIA in general and the HIPO team in particular. Years of work are now beginning to pay off as SOFIA flight operations are beginning. Long-awaited tests are being done to verify the performance of HIPO and to determine whether design decisions made 10-20 years ago to improve upon KAO capabilities are working as planned. HIPO is performing very well and SOFIA has the necessary capabilities to support our science goals. We are pursuing challenging new problems in aero-optics, precise photometry, occultation prediction, and flight operations, and look forward to many productive flights to come. SOFIA and HIPO are open for business!

ACKNOWLEDGEMENTS

The HIPO project is supported by USRA subcontract 8500-98-003. We thank USRA for their unwavering support for this project over the years and to Lowell Observatory and its staff for their forbearance as HIPO delayed other work at the Observatory. HIPO could not have been successfully completed without the support of the technical staff at Lowell, particularly Ralph Nye, Rich Oliver, and Steve Lauman. We thank Bill Rose for his continued interest in aero-optical issues and support of our undertakings. We owe a particular debt of gratitude to the late Jim Elliot and Jim Darwin. Jim Elliot was Co-Investigator on the HIPO project from its beginning until his death only a few months before our first flight. Jim Darwin, Lowell's instrument maker for many years, made most of the mechanical parts for HIPO as well as some of its mechanical designs. Jim passed away just weeks before our first flight.

REFERENCES

[1] Elliot, J.L., "Stellar Occultation Studies of the Solar System", *Ann. Rev. Astron. Astrophys.* **17**, 445-475 (1979).
[2] Charbonneau, D., T.M. Brown, A. Burrows, and G. Laughlin, "When Extrasolar Planets Transit Their Parent Stars", in Protostars and Planets V, University of Arizona Press, 701-716 (2007).
[3] Brown, T.M.., and R.L. Gilliland, "Asteroseismology", *Ann. Rev. Astron. Astrophys.* **32**, 37-82 (1994).
[4] Dunham, E.W., "The Optical Design of HIPO: A High-speed Imaging Photometer for Occultations", *Proc. SPIE* **4857**, 62-72, (2002).
[5] Dunham, E.W., J.L. Elliot, T.A. Bida, and B.W. Taylor, "HIPO – A High-speed Imaging Photometer for Occultations", Proc. SPIE 5492, 592-603 (2004).
[6] Dunham, E.W., J.L. Elliot, T.A. Bida, P.L. Collins, B.W. Taylor, and S. Zoonematkermani, "HIPO Data Products", Proc. SPIE 7014, 70144Z-1-70144Z-10 (2008).
[7] Dunham, E.W., Collins P.L., Reinacher A., Lampater U.,"SOFIA Image Motion Compensation," Proc SPIE 7735, 77355X, (2010).
[8] McLean, I. S., Smith, E. C., Aliado, T., Brims, G., Kress, E., Magnone, K.; Milburn, J, Oldag, A., Silvers, T., and Skulason, G., "FLITECAM, a 1-5 micron camera and spectrometer for SOFIA, " Proc. SPIE*,* 6269, 195 (2006).
[9] F. Harms, Wolf, J., Waddell, P., Dunham, E., Reinacher, A., Lampater, U., Jakob, H., Bjarke, L., Adams, S., Grashuis, R., Meyer, A., Bower, K., Schweikhard, K., and Keilig, T. "On sky testing of the SOFIA telescope in preparation for the first science observations", by, Proc. SPIE, 7453, 3-15 (2009).
[10] Pfüller, E., Wolf, J., Hall, H., and Röser, H-P., "Optical characterization of the SOFIA telescope using fast EM-CCD cameras", Proc. SPIE, 8444-38, this conference, (2012).
[11] McLean, I. S., Smith, E. C., Becklin, E. E.; Dunham, E. W., Milburn, J. W., and Savage, M. L., "FLITECAM: current status and results from observatory verification flights " Proc. SPIE*,* 8446-43, this conference, (2012).
[12] Keas, P. J., Dunham, E., Lampater, U., Pfüller, E., Röser, H-P., Wiedemann, M., and Wolf, J., "Active damping of the SOFIA Telescope Assembly", Proc. SPIE, 8444-36, this conference, (2012).
[13] Temi, P., et al., "SOFIA observatory performance and characterization", Proc. SPIE, 8444-39. this conference, (2012).
[14] Kärcher, H. J., "Airborne environment – a challenge for telescope design", Proc. SPIE, 4014, 278-284 (2000).
[15] Dunham, E.W., and J.L. Elliot, "Optical Photometry with the Kuiper Airborne Observatory", *Pub. A.S.P.* **95**, 325-331 (1983).
[16] Elliot, J.L., *et al.*, "Image Quality on the Kuiper Airborne Observatory. I. Results of the First Flight Series", Pub. A.S.P. 101, 737-764 (1989).
[17] Massey, P., K. Strobel, J.V. Barnes, and E. Anderson, "Spectrophotometric Standards", *Ap. J.* **328**, 315-333, 1988.
[18] Dravins, D., L. Lindegren, E. Mezey, and A.T. Young, "Atmospheric Intensity Scintillation of Stars. I. Statistical Distributions and Temporal Properties", *Pub. A.S.P.* **109**, 173-207 (1997).
[19] Rose, W. C., Private communication.